The Astronomical Journal, 137:3864–3868, 2009 April doi:10.1088/0004-6256/137/4/3864

HUBBLE SPACE TELESCOPE OBSERVATIONS OF AN EXTRAORDINARY FLARE IN THE M87 JET*

Juan P. Madrid[1]
Space Telescope Science Institute, 3700 San Martin Drive, Baltimore, MD 21218, USA
Received 2008 June 4; accepted 2009 January 14; published 2009 March 6

ABSTRACT

HST-1, a knot along the M87 jet located 0.″85 from the nucleus of the galaxy, has experienced dramatic and unexpected flaring activity since early 2000. We present analysis of *Hubble Space Telescope* near-ultraviolet (NUV) imaging of the M87 jet from 1999 May to 2006 December that reveals that the NUV intensity of HST-1 has increased 90 times over its quiescent level and outshines the core of the galaxy. The NUV light curve that we derive is synchronous with the light curves derived in other wavebands. The correlation of X-ray and NUV light curves during the HST-1 flare confirms the synchrotron origin of the X-ray emission in the M87 jet. The outburst observed in HST-1 is at odds with the common definition of active galactic nucleus variability usually linked to blazars and originating in close proximity to the central black hole. In fact, the M87 jet is not aligned with our line of sight and HST-1 is located at one million Schwarzchild radii from the supermassive black hole in the core of the galaxy.

Key words: galaxies: active – galaxies: individual (M87) – galaxies: jets

1. INTRODUCTION

M87, the cD galaxy of the Virgo cluster, is a giant elliptical famed for its spectacular galactic-scale plasma jet. Due to its proximity, images of M87's jet at high resolution have revealed a profusion of distinct knots or regions of enhanced emission along the whole length of the jet. These knots have been clearly detected at radio, optical, ultraviolet (UV), and X-ray wavelengths. The detection of these UV and X-ray emission regions, hundreds of parsecs away from the active galactic nucleus (AGN), proves that these are regions of in situ particle acceleration within the jet because such high-energy emission vanishes rapidly. The radiative half-lives of synchrotron X-ray emitting electrons are of the order of years and the cooling time for UV emitting particles are of the order of decades (Harris & Krawczynski 2006). High-energy emission would be confined in a small space without reacceleration along the jet. Thus, these knots must be regions of acceleration distinct from the AGN.

Until 2000 February HST-1 was an inconspicuous knot of the M87 jet located 0.″85 from the nucleus of the galaxy (Waters & Zepf 2005). Since that date, HST-1 has shown an unexpectedly rapid variability in all wavebands. More strikingly, in 2003 HST-1 became brighter than the nucleus of the galaxy, which is known to harbor a supermassive black hole of $3.2\pm0.9\times10^9\ M_\odot$ (Macchetto et al. 1997). HST-1 is also the most probable site of production of the TeV γ-rays emanating from M87, recently reported by the HESS collaboration (Aharonian et al. 2006; see also Cheung et al. 2007).

Specific observations of HST-1 have been carried out across the electromagnetic spectrum, and a particularly detailed study of the flaring of HST-1 has been conducted with the *Chandra* X-ray Observatory by D. E. Harris and collaborators (Harris et al. 2003, 2006, 2008). The X-ray intensity of this peculiar knot has increased more than 50 times in the past five years and peaked in 2005. There is a wealth of high-quality *Hubble Space Telescope* (*HST*) near-ultraviolet (NUV) imaging data of the M87 jet that has been only succinctly presented in the past (Madrid et al. 2007). The NUV light curve for HST-1 that we present here has broadly the same shape as the X-ray light curve presented by Harris et al. (2006): the flare rises, peaks, and declines simultaneously in the X-rays and the NUV.

HST-1 is located at one million Schwarzchild radii away from the galactic nucleus but if M87 were at a greater distance, or if our telescopes had lesser resolution, this flare would have been interpreted as variability intrinsic to the central black hole and its immediate vicinity. This blazar-like behavior is clearly isolated from the central engine and it is not directly beamed as the M87 jet is misaligned with respect to the line of sight (LOS; Harris et al. 2006; Cheung et al. 2007). A detailed characterization of this flare is thus important to better understand blazar variability.

We describe the *HST* view of the remarkable flaring of the HST-1 knot with high-resolution imaging taken over more than seven years of observations and aim to present the visually striking NUV data that bridge the gap between the X-ray (Harris et al. 2006) and radio (Cheung et al. 2007) observations of HST-1.

2. OBSERVATIONS AND DATA REDUCTION

We present observations obtained with two instruments on board the *HST*: the Space Telescope Imaging Spectrograph (STIS) and the Advanced Camera for Surveys (ACS).

The STIS stopped functioning in 2004 August due to an electronics failure on the redundant (side 2) power supply system. All observations after 2004 August were taken with the ACS. Even though each of these two instruments has unique characteristics, they cover the same wavebands and provide data that are easily compared. Moreover, the ACS images have the same file structure as STIS images, making the data reduction procedure very similar between the two instruments. The discrepancy between the STIS and the ACS absolute photometric calibration does not exceed 2% (Bohlin 2007).

The STIS observations were carried out using the NUV/Multianode Microchannel Array (MAMA) detector which has a field of view (FOV) of 24.″7 × 24.″7 and a pixel size of 0.″024. The M87 jet was imaged with the F25QTZ filter that has its

* Based on observations made with the NASA/ESA *Hubble Space Telescope*, obtained at the Space Telescope Science Institute, which is operated by the Association of Universities for Research in Astronomy, Inc., under NASA contract NAS 5-26555. These observations are associated with programs 9474, 10133, 10617.
[1] Now at Department of Physics and Astronomy, McMaster University, Hamilton, ON L8S 4M1, Canada.

maximum throughput a wavelength at 2364.8 Å and a width of 995.1 Å. Due to the nature of the detector NUV/MAMA, images are free of cosmic rays (Kim Quijano et al. 2003).

The ACS High-Resolution Camera (HRC) is a CCD instrument with an FOV of $29'' \times 25''$ and a scale of $\sim 0\farcs025$ per pixel. We analyze images acquired with the F220W and F250W filters, which are the two broadband NUV filters with the most similar characteristics to the STIS F25QTZ filter. The F220W filter has its pivot wavelength at 2255.5 Å and a width of 187.3 Å; for F250W, these values are 2715.9 Å and 239.4 Å, respectively (Mack et al. 2003; Gonzaga et al. 2005).

We obtained the flat-fielded science files (FLT) from the *HST* public archive for data acquired by both instruments. These science-ready files are processed through the automatic reduction and calibration pipeline (CALACS) before they are retrieved from the public archive. The pipeline subtracts the bias and dark current and applies the flat field to the raw CCD data (Sirianni et al. 2005). Subsequent data reduction was performed using the software package Space Telescope Science Data Analysis System (STSDAS).

We analyzed data taken over a period of time of more than seven years, from 1999 May through 2006 December. Each image, at all epochs, is the product of the combination of four single exposures taken within the same orbit. This allows us to eliminate cosmic rays in the ACS images and improve the signal to noise.

We used the STSDAS task MULTIDRIZZLE to apply the geometric distortion correction, eliminate cosmic rays, and align and combine the individual exposures of every epoch. The distortion correction was computed with up-to-date distortion coefficient tables retrieved from the Multimission Archive at the Space Telescope (MAST). During the data reduction process, we preserved the native pixel size. The final output images generated by MULTIDRIZZLE have units of counts per second for the STIS data and units of electrons per second for the ACS data (Koekemoer et al. 2002).

We derive fluxes and errors by doing aperture photometry with PHOT and an aperture radius of 10 pixels or $0\farcs25$. At the distance of M87, 16.1 Mpc (Tonry et al. 2001), $1''$ corresponds to 77 pc. We convert the number of counts obtained with PHOT into flux and flux errors by using PHOTFLAM, or inverse sensitivity, for each instrument found in the updated ACS zeropoint tables maintained by the STScI, or in the header of the STIS images:

$$\mathrm{PHOTFLAM_{STIS/F25QTZ}} = 5.8455.10^{-18}\ \mathrm{erg\ cm^{-2}\AA}$$
$$\mathrm{PHOTFLAM_{ACS/F220W}} = 8.0721.10^{-18}\ \mathrm{erg\ cm^{-2}\AA}$$
$$\mathrm{PHOTFLAM_{ACS/F250W}} = 4.7564.10^{-18}\ \mathrm{erg\ cm^{-2}\AA}.$$

Once the calibrated fluxes and Poisson errors are derived, they are transformed into millijanskys using the pyraf task CALCPHOT of the synthetic photometry (SYNPHOT) software package under STSDAS. We also scale the flux measurements obtained with different bands using SYNPHOT (Laidler et al. 2005). We expect that no additional errors are introduced by SYNPHOT when doing the transformation to millijanskys. We assume that the spectrum of HST-1 is described by a power law with index α (Perlman et al. 2001), and we define the flux density as $S_\nu \propto \nu^{-\alpha}$.

The background light was estimated by measuring the flux with the same circular aperture at the same radial distance from the nucleus than HST-1, but on the side of the jet. The aperture corrections were performed using the values published by Proffitt et al. (2003) for STIS and Sirianni et al. (2005) for the ACS. We use the reddening toward M87 determined by Schlegel et al. (1998), $E(B-V) = 0.022$, and the extinction relations from Cardelli et al. (1989) to derive the extinction in the *HST* filters. We find the following values for the extinction: $A_{\mathrm{F25QTZ}} = 0.190$, $A_{\mathrm{F220W}} = 0.220$, and $A_{\mathrm{F250W}} = 0.134$.

3. RESULTS

HST-1 was dormant until 2000 February when its flaring activity began (Waters & Zepf 2005). We see this in Figure 1, which is a zoom of the inner regions of the M87 jet and displays, on the left, the early evolution of HST-1. Three main emission loci are visible in this zoom, from left to right; these are the nucleus of the galaxy, HST-1, and knot D, respectively. The images in the left column of Figure 1 were acquired with STIS/F25QTZ while the images on the right column were taken with the ACS in the F220W band.

In the STIS image of 1999 May (top left), HST-1 was an unremarkable knot along the M87 jet. The brightening of HST-1 is already noticeable in 2001 July. The images in the lower left were taken in 2002 February and 2002 July, respectively, and show the slow brightening of HST-1 during this year. At the end of 2002, HST-1 is 15 times brighter than in 1999 May.

In 2003, HST-1 became dramatically variable. The image on the top right was taken in 2003 April as HST-1 continues to rise in flux. HST-1 is at its highest recorded brightness in 2005 May; on this date, we recorded the highest flux of HST-1 in the NUV, namely 0.54 mJy. At this point in time, the NUV flux of HST-1 was four times the measured flux of the central engine of the galaxy. The peak of the X-ray flux based on *Chandra* observations was reported on 2005 April (Harris et al. 2006). HST-1 attained an NUV flux, 90 times its quiescent level in 2005 May. The *HST* data acquired in 1999 give us a measure of the brightness of HST-1 during its latent state and allow us to measure the total factor by which the brightness changed during the outburst. *Chandra* was just launched in 1999 and very long baseline interferometry (VLBI) radio observations date back to 2000 only (Cheung et al. 2007).

After May 2005, HST-1 declined in intensity with a decay time similar to the rise time. HST-1 experienced a second and also unexpected outburst in 2006 November. This second outburst is fainter than the first one in 2005 May. The image on the lower right of Figure 1 shows HST-1 during the second, yet fainter, outburst in 2006 November. It is evident from Figure 1 that the jet itself is better mapped by the STIS images.

Table 1 presents the log of observations of the M87 jet taken with the STIS and ACS. This table also presents the NUV intensities and Poisson errors of the nucleus of the galaxy and HST-1 at all epochs studied here. Although magnitudes of the Space Telescope system or erg $\mathrm{s^{-1}\ cm^{-2}\ Hz^{-1}}$ would be more natural units, we decided to plot our light curve in mJy to facilitate comparison with observations at other wavebands (Waters & Zepf 2005; Perlman et al. 2003; Harris et al. 2006).

Figure 2 shows the light curve of HST-1 and the nucleus of the galaxy. The HST-1 light curve is bumpy in the radio and the X-rays and the NUV is not an exception. The dramatic flaring of HST-1 can be clearly appreciated in this figure.

Table 2 contains the doubling time (DT) and halving time (HT) for HST-1 calculated for the NUV following the prescriptions of Harris et al. (2006). We calculate $y = I_2/I_1$, the flux ratio, and the time elapsed, Δt, between two consecutive observations. The DT is calculated using $\mathrm{DT}=[\frac{1}{y-1}]\Delta\mathrm{t}$ and the HT by $\mathrm{HT}=[\frac{0.5}{1-y}]\Delta\mathrm{t}$. The bumpiness attributed to synchrotron losses in

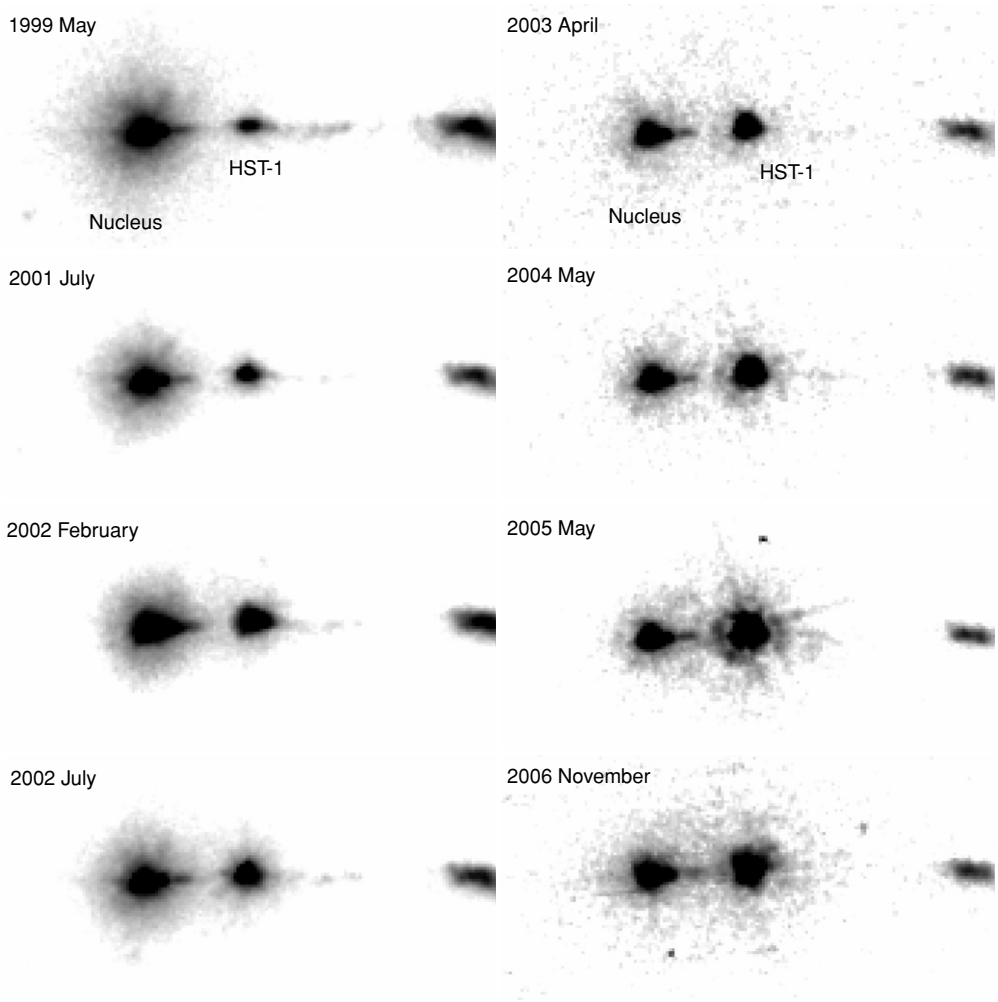

Figure 1. Observations of the inner jet of M87 taken with the STIS/F25QTZ (left column) and the ACS/F220W (right column). The nucleus is on the left; HST-1 is the variable feature to the right as noted on the top image of each column. The observation date is on the upper left-hand corner of each image. The total jet length shown in these images is about 3″ or 230 pc. The jet has been rotated to be aligned with the horizontal axis.

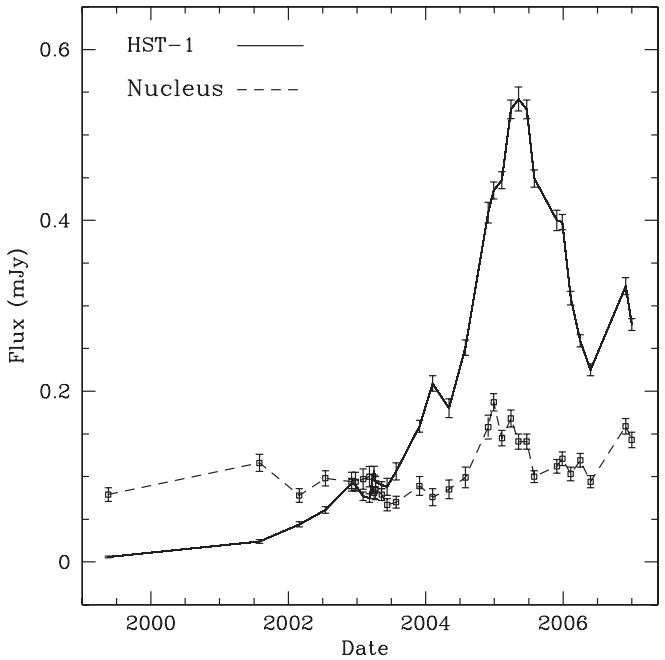

Figure 2. NUV light curve for knot HST-1 and the nucleus of M87 from 1999 May to 2006 December, in units of millijanskys (mJy), 1 Jy = 10^{-26} W Hz^{-1} m^{-2}.

the X-ray persists in the NUV. These rapid variations of brightness are consistent with the month timescale variability reported by Perlman et al. (2003) for the early stages of the flare and are found here to persist through time.

The X-ray and NUV light curves of HST-1 are plotted together in Figure 3. We performed a formal correlation analysis of these two light curves by taking 30 simultaneous values of the NUV and X-ray fluxes and deriving the Spearman rank correlation coefficient ρ. This coefficient is a nonparametric measure of correlation and the range is $0 < \rho < 1$; the higher the value, the more significant the correlation (Wall & Jenkins 2003). Simultaneous measurements of the flux of HST-1 in the X-ray and the NUV yield $\rho = 0.966$ reflecting a strong correlation.

4. DISCUSSION

In Harris et al. (2003), synchrotron loss models based on the NUV data available at that time predicted the optical decay time of the flare to be a factor of 10 larger than the X-ray decay time. On the other hand, Perlman et al. (2003) forethought a similar decay timescale for both optical and X-ray light curves.

The simultaneous rise and fall of the flare at NUV and X-ray wavelengths support the first plausible hypothesis of the physical origin of the HST-1 flare postulated by Harris et al. (2006), namely that a simple compression caused the

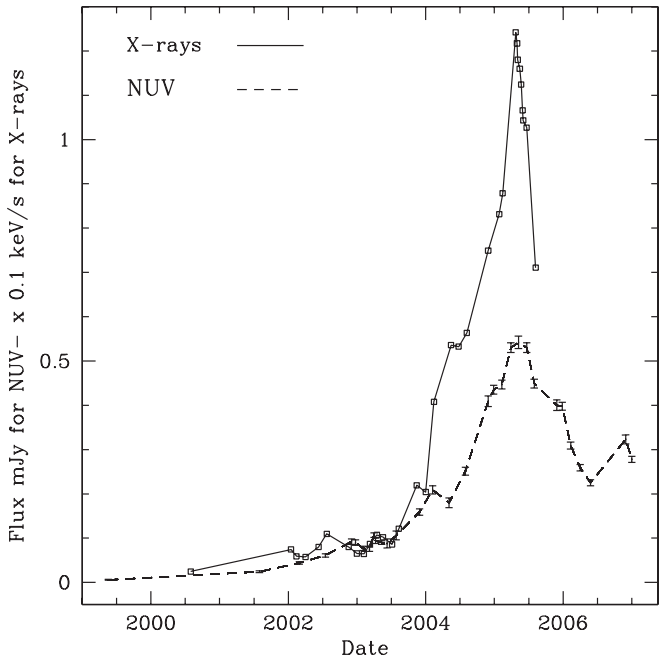

Figure 3. NUV and X-ray light curves of HST-1. The X-ray data were taken from Harris et al. (2006).

Table 1
Log of Observations and NUV Intensities of the Nucleus and HST-1

Date	Camera/Filter	Nucleus	HST-1
1999 May 17	STIS/F25QTZ	0.079 ± 0.008	0.006 ± 0.001
2001 Jul 30	STIS/F25QTZ	0.116 ± 0.010	0.024 ± 0.002
2002 Feb 27	STIS/F25QTZ	0.078 ± 0.008	0.044 ± 0.003
2002 Jul 17	STIS/F25QTZ	0.098 ± 0.009	0.061 ± 0.004
2002 Nov 30	ACS/F220W	0.094 ± 0.011	0.092 ± 0.006
2002 Dec 22	ACS/F220W	0.094 ± 0.011	0.090 ± 0.006
2003 Feb 2	ACS/F220W	0.097 ± 0.012	0.077 ± 0.005
2003 Mar 6	ACS/F220W	0.100 ± 0.012	0.075 ± 0.005
2003 Mar 31	ACS/F250W	0.081 ± 0.007	0.107 ± 0.005
2003 Apr 7	ACS/F220W	0.084 ± 0.011	0.094 ± 0.006
2003 May 10	ACS/F250W	0.079 ± 0.007	0.090 ± 0.004
2003 Jun 7	STIS/F25QTZ	0.067 ± 0.007	0.088 ± 0.010
2003 Jul 27	STIS/F25QTZ	0.070 ± 0.007	0.106 ± 0.010
2003 Nov 29	ACS/F220W	0.089 ± 0.011	0.159 ± 0.007
2004 Feb 7	ACS/F220W	0.076 ± 0.010	0.209 ± 0.009
2004 May 5	ACS/F220W	0.085 ± 0.011	0.180 ± 0.011
2004 Jul 30	ACS/F220W	0.099 ± 0.012	0.251 ± 0.009
2004 Nov 28	ACS/F220W/F250W	0.158 ± 0.014	0.409 ± 0.012
2004 Dec 26	ACS/F250W	0.187 ± 0.010	0.435 ± 0.010
2005 Feb 9	ACS/F250W	0.145 ± 0.009	0.447 ± 0.010
2005 Mar 27	ACS/F250W	0.168 ± 0.010	0.530 ± 0.011
2005 May 9	ACS/F220W/F250W	0.141 ± 0.009	0.542 ± 0.014
2005 Jun 22	ACS/F250W	0.141 ± 0.009	0.530 ± 0.011
2005 Aug 1	ACS/F250W	0.100 ± 0.007	0.449 ± 0.010
2005 Nov 29	ACS/F220W/F250W	0.112 ± 0.008	0.400 ± 0.012
2005 Dec 26	ACS/F250W	0.121 ± 0.008	0.398 ± 0.009
2006 Feb 8	ACS/F220W/F250W	0.103 ± 0.008	0.309 ± 0.008
2006 Mar 30	ACS/F250W	0.119 ± 0.008	0.259 ± 0.007
2006 May 23	ACS/F220W/F250W	0.094 ± 0.007	0.225 ± 0.007
2006 Nov 28	ACS/F220W/F250W	0.159 ± 0.009	0.323 ± 0.010
2006 Dec 30	ACS/F250W	0.143 ± 0.009	0.278 ± 0.007

Notes. Column 1: observation dates; Column 2: camera and filter in use; Column 3: nucleus flux and Poisson error in millijanskys; Column 4: flux and Poisson error for HST-1 in millijanskys.

Table 2
NUV DT and HT for HST-1

Epoch Interval	Δt	$y-1$	DT	HT
1999 May 17–2001 Jul 30	2.21	3.00	0.73	
2001 Jul 30–2002 Feb 27	0.58	0.83	0.70	
2002 Feb 27–2002 Jul 17	0.38	0.39	0.97	
2002 Jul 17–2002 Nov 30	0.37	0.51	0.72	
2002 Nov 30–2002 Dec 22	0.06	0.02		1.50
2002 Dec 22–2003 Feb 02	0.12	0.14		0.43
2003 Feb 2–2003 Mar 6	0.09	0.03		1.50
2003 Mar 6–2003 Mar 31	0.07	0.43	0.16	
2003 Mar 31–2003 Apr 7	0.02	0.12		0.08
2003 Apr 7–2003 May 10	0.09	0.04		1.13
2003 May 10–2003 Jun 7	0.08	0.22		0.18
2003 Jun 7–2003 Jul 27	0.14	0.21	0.67	
2003 Jul 27–2003 Nov 29	0.34	0.50	0.68	
2003 Nov 29–2004 Feb 7	0.19	0.31	0.61	
2004 Feb 7–2004 May 5	0.24	0.14		0.85
2004 May 5–2004 Jul 30	0.24	0.39	0.61	
2004 Jul 30–2004 Nov 28	0.33	0.63	0.52	
2004 Nov 28–2004 Dec 26	0.08	0.06	1.33	
2004 Dec 26–2005 Feb 09	0.12	0.03	4.44	
2005 Feb 9–2005 Mar 27	0.12	0.19	0.63	
2005 Mar 27–2005 May 9	0.12	0.02	5.22	
2005 May 9–2005 Jun 22	0.12	0.02		5.22
2005 Jun 22–2005 Aug 1	0.11	0.15		0.36
2005 Aug 1–2005 Nov 29	0.33	0.11		1.50
2005 Nov 29–2005 Dec 26	0.07	0.01		3.50
2005 Dec 26–2006 Feb 8	0.12	0.22		0.27
2006 Feb 8–2006 Mar 30	0.14	0.16		0.44
2006 Mar 30–2006 May 23	0.15	0.13		0.57
2006 May 23–2006 Nov 28	0.52	0.44	1.18	
2006 Nov 28–2006 Dec 30	0.09	0.14		0.32

Notes. Column 1: dates; Column 2: Δt time interval in years; Column 3: $y-1$, where $y=I_2/I_1$, $1-y$ if $I_2 < I_1$; Column 4: DT or HT.

HST-1 outburst. Compression increases both the magnetic field strength and the particle energy at all wavelengths equally, leading to simultaneous flaring at all wavebands. The magnetic field vectors in HST-1 are perpendicular to the jet direction also consistent with a shock (Perlman et al. 2003).

The overall rise and fall timescales, similar in both bands, and the lack of a large delay between bands suggest a rapid expansion as a probable cause for the decrease in luminosity. However, a more rigorous analysis of the rise and fall timescales shows that expansion is not the dominant mechanism of energy loss for HST-1, see below (Harris et al. 2008).

A more elaborated theoretical interpretation for the origin of HST-1 was presented by Stawarz et al. (2006) and supported by the observations of Cheung et al. (2007). This newer hypothesis claims that HST-1 originates in a nozzle throat of the M87 jet that creates reconfinement of magnetic field lines liberating large amounts of energy, similar to the process responsible for solar flares. The gravitational influence of the central AGN on the velocity dispersion of the stars in the innermost regions of this galaxy has been well documented with early *HST* observations (Lauer et al. 1992; see also Macchetto et al. 1997). The hot thermal gas can be expected to follow the distribution of the stars in this inner region and create a reconfinement shock in the jet due to an enhanced thermal pressure. This reconfinement should happen at roughly the same distance of the well-known stellar cusp, precisely where HST-1 lies (Stawarz et al. 2006).

The doubling and halving timescales of the NUV presented in this paper and the X-rays ones published by Harris et al. (2006) do not always perfectly overlap in time; the *HST* and *Chandra* observations were not taken simultaneously. However,

it is evident from the values of Table 2 and the values of Tables 3 and 6 of Harris et al. (2006) that the rise and fall timescales are consistently larger in the NUV than in the X-rays. See, for instance, the time interval between 2005 June 21 and 2005 August 6 when the HT for the X-rays is 0.21 while in the NUV between 2005 June 22 and 2005 August 1, the HT is 0.36. Harris et al. (2008) made a detailed analysis of rise and fall timescales for HST-1 and concluded that this longer decay time in the NUV is an indication that expansion is not the primary energy loss mechanism for the charged particles emitting within the HST-1 region.

The detection of polarized emission as well as synchrotron emission models fitted to flux measurements provided evidence that the physical process responsible for the radio-to-UV emission in the knots of the M87 jet is synchrotron radiation of electrons accelerated by the magnetic field of the jet (Perlman et al. 2001). The very strong correlation between the NUV and X-ray light curves of the HST-1 flare proves that the same physical phenomenon and the same electrons are responsible for the emission in both bands. Therefore, the X-ray emission is also synchrotron in origin. The injection of fresh particles into the flaring volume is not needed to explain the high-energy emission; the X-ray emission is well interpreted as the high-energy extension of the radio to optical spectrum (Perlman & Wilson 2005; Harris et al. 2006). The observations presented here rule out inverse Compton (IC) up-scattering of lower energy electrons, as the cause of the high-energy emission of this flare in particular, and of the other emission knots along the M87 jet. Moreover, high-energy photons produced by IC up-scattering would take much longer (10,000 years) than the time observed to decrease in flux (Harris 2003). We can thus safely state that synchrotron emission is the physical process responsible for the high-energy emission in the M87 jet.

The encircled energy distribution of HST-1 follows the pattern of the detectors' point-spread function (PSF) at all epochs. In the NUV, HST-1 remains unresolved with an upper limit on its size of $\sim 0\farcs025$, that is, $\sim$1.9 pc.

The HESS collaboration recently reported a detection of TeV γ-rays emanating from M87, but the Cherenkov telescopes used for this detection lack the resolution to determine the exact position of the TeV emitting region. Cheung et al. (2007) favored HST-1 over the nucleus as the site of origin of the TeV emission. They noted that the light curve of TeV emission in M87 is roughly similar to the light curve of the HST-1 flare seen in the radio and X-ray. The NUV peaks simultaneously with the X-rays and the γ-rays, and only HST-1 shows a flaring behavior in the NUV. The nucleus shows only the characteristic low amplitude variability (see Figure 2). These facts support the hypothesis of HST-1 as the site of origin of the γ-rays through the IC up-scattering of ambient photons by high-energy electrons produced during the outburst.

After 2003 May, and for more than four years, the flux of HST-1 dominated the NUV emission of M87, patently overpowering the emission of the central engine (see Figure 3). Given that within radio galaxies the principal sources of particle acceleration are the core and the jet, the large flux from this flare plays, as we have shown here, a crucial role in determining the NUV flux and therefore the spectrum of the entire galaxy.

As part of the *Chandra* Cen A Very Large Project, Hardcastle et al. (2007) searched, to no avail, for HST-1-like variability in the X-ray jet of this galaxy (D=3.7Mpc). Hardcastle et al. aimed at answering an important question: is HST-1 a feature unique of M87? Or is this extreme variability ubiquitous, or at least frequent, in AGN jets? If an HST-1-type outburst occurred in a more distant AGN, it would not be resolved with current optical and X-ray instruments and would probably be associated with Doppler boosting of emission emanating from a jet close to the LOS or with events associated with the variability of the accretion disk of the black hole. However, the angle of the M87 jet with the LOS is about 26°–30° (Cheung et al. 2007; Bicknell & Begelman 1996) allowing only a modest beaming. Also, given its large distance from the core (that is, more than 65 pc or one million Schwarzchild radii) intrinsic black hole variability has no direct relation with this flaring. Outbursts similar to HST-1 can be responsible for variability associated with high redshift blazars but remain completely unresolved.

This research has made use of the NASA Astrophysics Data System Bibliographic services. I wish to thank J. Mack and M. Sirianni (STScI) for answering an endless list of questions about the ACS. I am grateful to E. Vishniac (McMaster) for believing in my understanding of accretion disks. The anonymous referee gave a very constructive report that helped to improve this paper. L. Schwartz (JHU) encouraged me to carry out this project and many others.

REFERENCES

Aharonian, F., et al. 2006, Science, 314, 1424
Bicknell, G. V., & Begelman, M. C. 1996, ApJ, 467, 597
Bohlin, R. C. 2007, Photometric Calibration of the ACS CCD Cameras, ACS Instrument Science Report 2007-06 (Baltimore, MD: STScI)
Cardelli, J. A., Clayton, G. C., & Mathis, J. S. 1989, ApJ, 345, 245
Cheung, C., Harris, D. E., & Stawarz, L. 2007, ApJ, 663, L65
Gonzaga, S., et al. 2005, ACS Instrument Handbook, Version 6.0 (Baltimore, MD: STScI)
Hardcastle, M. J., et al. 2007, ApJL, 670, L81
Harris, D. E. 2003, New Astron. Rev., 47, 617
Harris, D. E., Biretta, J. A., Junor, W., Perlman, E. S., W. B., Sparks, W., & Wilson, A. S. 2003, ApJ, 586, L41
Harris, D. E., Cheung, C. C., Biretta, J. A., Sparks, W. B., Junor, W., Perlman, E. S., & Wilson, A. S. 2006, ApJ, 640, 211
Harris, D. E., Cheung, C. C., Stawarz, L., & Perlman, E. S. 2008, submitted
Harris, D. E., & Krawczynski, H. 2002, ApJ, 565, 244
Harris, D. E., & Krawczynski, H. 2006, ARA&A, 44, 463
Kim Quijano, J., et al. 2003, STIS Instrument Handbook, Version 7.0 (Baltimore, MD: STScI)
Koekemoer, A. M., Fruchter, A. S., Hook, R. N., & Hack, W. 2002, in The 2002 *HST* Calibration Workshop: Hubble after the Installation of the ACS and the NICMOS Cooling System, ed. S. Arribas, A. Koekemoer, & B. Whitmore (Baltimore, MD: STScI), 339
Laidler, V., et al. 2005, Synphot User's Guide, Version 5.0 (Baltimore, MD: STScI)
Lauer, T. R., et al. 1992, AJ, 103, 703
Macchetto, F. D., et al. 1997, ApJ, 489, 579
Mack, J., et al. 2003, ACS Data Handbook Version 2.0 (Baltimore, MD: STScI),
Madrid, J. P., Sparks, W. B., Harris, D. E., Perlman, E. S., Macchetto, D., & Biretta, J. 2007, Ap&SS, 311, 329
Perlman, E. S., Biretta, J. A., Sparks, W. B., Macchetto, F. D., & Leahy, J. P. 2001, ApJ, 551, 206
Perlman, E. S., Harris, D. E., Biretta, J. A., Sparks, W. B., & Macchetto, F. D. 2003, ApJ, 599, L65
Perlman, E. S., & Wilson, A. S. 2005, ApJ, 627, 140
Proffitt, C. R., Brown, T. M., Mobasher, B., & Davies, J. 2003, Instrument Science Report, STIS 2003-01 (Baltimore, MD: STScI)
Schlegel, D. J, Finkbeiner, D. P., & Davis, M. 1998, ApJ, 500, 525
Sirianni, M., et al. 2005, PASP, 117, 1049
Stawarz, L., et al. 2006, MNRAS, 370, 981
Ulrich, M. E., Marashi, L., & Urry, C. M. 1997, ARA&A, 35, 445
Tonry, J. L., et al. 2001, ApJ, 546, 681
Wall, J. V., & Jenkins, C. R. 2003, Practical Statistics for Astronomers (Cambridge: Cambridge Univ. Press)
Waters, C. Z., & Zepf, S. E. 2005, ApJ, 624, 656